Experimental Mechanics (2007) 47: 153–161
DOI 10.1007/s11340-006-7906-2

Shell Buckling of Imperfect Multiwalled Carbon Nanotubes—Experiments and Analysis

P.R. Guduru · Z. Xia

Received: 21 November 2005 / Accepted: 23 February 2006 / Published online: 1 May 2006

Abstract Experiments were conducted in which multiwalled carbon nanotubes were subjected to uniaxial compression and shell-buckling loads were measured. A comparison with existing theoretical models shows that the predictions are about 40–50% smaller than the experimentally measured buckling loads. This is in contrast to the classical elastic shell studies in which the experimental values were always substantially lower than the predicted values due to imperfection sensitivity. It is proposed that the discrepancy between the predicted and measured value might be due to imperfections in the multiwalled nanotubes in the form of sp^3 bonds between the tube walls, which introduce shear coupling between them. An analytical model is presented to estimate the effect of the shear coupling on the critical buckling strain, which shows that the contribution from shear coupling increases linearly with the effective shear modulus between the walls. Further, this contribution increases with the number of walls; the increment from each additional wall progressively decreases.

Keywords Carbon nanotube · Shell buckling · Shear coupling · Nanoindentation · sp^3 bonds

Introduction

Although there have been several previous studies in manipulating carbon nanotubes and deforming them to measure their mechanical properties [1–7], there have been few experimental studies on their uniaxial compression and buckling. One of the reasons is the difficulty of achieving well aligned axial loading on such small structures. When the nanotubes are long $[(L/R)^2 > \pi^2 R\sqrt{3(1-\nu^2)}\big/2h$, where L and R are the length and radius, respectively. ν is the Poisson's ratio and h is the wall thickness], axial compression results in "Euler" or "column" buckling. When they are short (replacing > with < in the above inequality), they are expected to undergo "shell" buckling, a common failure mode displayed by thin walled cylindrical structures. Although both types of nanotube buckling have been studied computationally [8–12], there exists only one experimental study of the "Euler" buckling of nanotubes [13], in which sophisticated nanomanipulation stages, combined with *in situ* scanning electron microscopy (SEM), were used to compress and observe long nanotubes. In that study, the emphasis was more on the nanomanipulation technique than on a systematic study of the mechanics of buckling. The only experimental investigation of shell buckling in nanotubes in compression has been reported recently by the authors [14, 15], in which individual and small groups of multiwalled carbon nanotubes were compressed in a nanoindenter. A summary of these experiments is presented in the next section, along with a discussion on the discrepancy between the measured buckling loads and the predicted values.

Experimental Observations

An experimental technique has been developed to compress individual, well-characterized multiwalled carbon nanotubes, using nanoindentation and study

P.R. Guduru (✉, SEM member) · Z. Xia
Division of Engineering,
Brown University, Providence, RI 02912, USA
e-mail: Pradeep_Guduru@Brown.edu

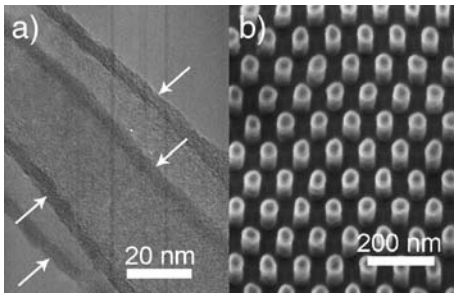

Fig. 1. Sample images. (**a**) Transmission electron microscopy image of multiwalled carbon nanotubes used in the experiments. From these images, the wall thickness is estimated to be 5 nm, which translates to 15 walls, assuming that the inter-wall spacing is 0.34 nm. (**b**) Scanning electron microscopy image of the *top (plan) view* of ordered nanotube array used in experiments

shell buckling. The multiwalled carbon nanotubes used in the current experiments were fabricated by the alumina template growth technique developed by Li et al. [16]. This method results in highly ordered and vertically aligned arrays of nanotubes of equal height, embedded in an alumina matrix. To generate a template for nanotube growth, a high purity aluminum foil is anodized in a multi-step process to create an alumina film with a self-organized hexagonal array of vertical nanopores. A cobalt catalyst is then electrodeposited at the bottom of the nanopores, followed by acetylene pyrolysis, which results in the growth of multiwalled carbon nanotubes along the length of the pores. This process results in highly ordered arrays of uniform nanotubes, the diameter of which can be controlled by changing the nanopore size between 20 and 200 nm. The wall thickness of the nanotubes was determined from transmission electron microscopy images [Fig. 1(a)] and the measured thickness of 5 nm corresponds to approximately 15 walls, taking the inter-wall spacing to be 0.34 nm. The nanotubes used in this study had 50 nm outer diameter, 40 nm inner diameter and were spaced at 100 nm, as shown in Fig. 1(b). A forest of vertically standing, aligned nanotubes is then obtained by etching the alumina matrix by any desired depth. Experiments were carried out on two sets of samples, on which the exposed heights of the nanotubes were 100 and 50 nm, respectively. These relatively short lengths ensure that compressive loading will cause shell buckling rather than column buckling in the nanotubes. The advantages of using such samples are that the need to manipulate individual nanotubes during testing is eliminated and that they facilitate easy vertical alignment with the nanoindenter tip. Thus, these samples are ideally suited for axial compression experiments.

Compression experiments on individual nanotubes are facilitated by the fine force and displacement resolutions (~300 nN and ~1 nm, respectively) available in a commercial nanoindenter (TriboIndenter, Hysitron, Minneapolis, MN). A Berkovich three-sided pyramidal tip was used, with a nominal tip radius of 100 nm. The experimental details of a single nanotube compression event are schematically illustrated in Fig. 2(a)–(b). During the experiment, individual nanotubes on the sample are located through in situ scanning to generate topography maps of the sample surface with the indenter tip, similar to atomic force microscopy (AFM). The image resolution is sufficient to locate the nanotubes unambiguously [Fig. 2(c)]. The scan area is typically 0.5×0.5 μm^2. After an image is obtained, the indenter tip is instructed to compress an individual nanotube. During compression, force and tip displacement are recorded. Immediately after a nanotube is indented, the same 0.5×0.5 μm^2 area of the surface is

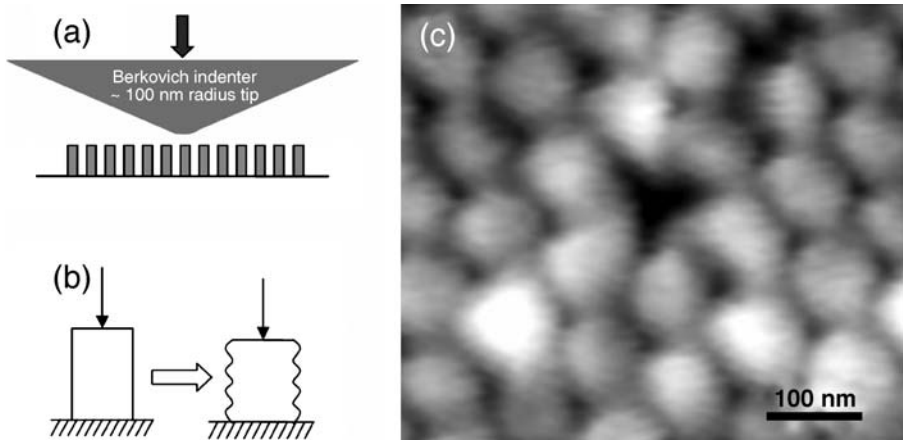

Fig. 2. Nanoindentation of individual carbon nanotubes. (**a**) Schematic illustration of the experiment in which a Berkovich indenter with 100 nm tip radius vertically compresses a multiwalled carbon nanotube. (**b**) Schematic illustration of shell buckling in nanotubes, which results in a load collapse and severe distortion of the nanotube walls. (**c**) An *in situ* scanning image of the sample surface obtained immediately after compressing a nanotube, by using the indenter tip as the scanning probe. The buckled nanotube is shorter than the neighboring nanotubes, resulting in a *dark triangular spot* in the topographic image

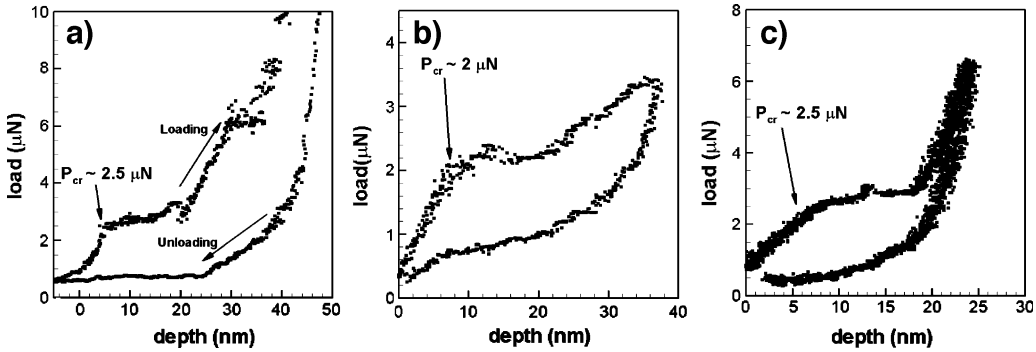

Fig. 3. Representative load–displacement data from a loading–unloading cycle. (**a**) Displacement-controlled indents on individual 100 nm long nanotubes, (**b**) load-controlled indents on individual 100 nm long nanotubes and (**c**) load-controlled indents on individual 50 nm long nanotubes. In all cases, buckling, evident by a distinct *drop in slope*, occurs between 2–2.5 μN. The critical buckling load was repeatable to within ±0.25 μN between experiments

imaged again to verify that the indentation was performed on the targeted nanotube, and not between nanotubes. An image taken after a successful indent is shown in Fig. 2(c), which shows the location of the buckled nanotube as a dark triangle in the hexagonal array of nanotubes; the neighboring nanotubes remain undisturbed.

The load–displacement curves obtained in three sets of experiments are shown in Fig. 3, in which each plot represents a loading–unloading cycle. The loading portion consists of three stages: an initial approximately linear increase, followed by a sudden drop in the slope and the curve becoming flat, and a third stage comprising an increasing load. The sudden decrease in the slope is the signature of shell buckling, which indicates the collapse process illustrated in Fig. 2(b). The critical buckling load has been consistently measured to be between 2 and 2.5 μN from multiple experiments. After buckling, neighboring nanotubes as well as the substrate come into contact with the indenter tip, which results in an increase in load, as seen in Fig. 3 in the third stage. In each plot, the position of zero displacement corresponds to a non-zero load because a small pre-load was used to detect the location of the sample surface. In order to image the buckled nanotubes, a 10 μm radius spherical indenter was used to buckle a large number of nanotubes, as illustrated in Fig. 4(a). Here, the indenting surface is "practically" flat at the scale of individual nanotubes and all nanotubes located near the center of the indent undergo shell buckling. The indent [Fig. 4(b)] is then easily located in SEM and an image of the buckled nanotubes is shown in Fig. 4(c). The buckled nanotubes have undergone distortion of cross-section and the walls are severely distorted and wrinkled, consistent with shell buckling modes observed in macroscopic elastic cylindrical shells [17]. These experiments clearly demonstrate that the high force and displacement resolutions available with commercial nanoindentation equipment can be exploited to perform nanoscale mechanical tests on individual multiwalled nanotubes and obtain repeatable data. It must be noted that the experimental data does not provide an independent measurement

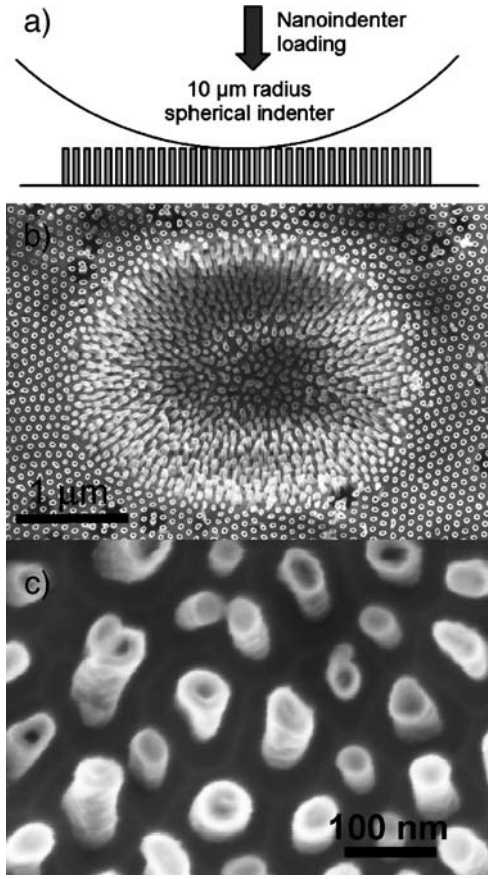

Fig. 4. Buckled nanotube images. (**a**) Schematic illustration of a 10 μm radius sphere indenting the nanotubes. (**b**) Scanning electron micrograph of the *top view* of a population of compressed nanotubes. (**c**) A *magnified view* of the buckled nanotubes showing distorted cross-sections and highly deformed and wrinkled side walls

of the critical buckling strain of the nanotubes, because of substrate and indenter compliance. However, this additional compliance does not affect the measured buckling loads; and hence buckling load is the only legitimate measurement from these experiments.

Comparison with Existing Models

For a thin-walled isotropic shell, the critical buckling strain from continuum theory is given by [18]

$$\varepsilon_{cr} = \frac{h}{R\sqrt{3(1-\nu^2)}} \tag{1}$$

where E is the elastic modulus, R the shell radius, h the shell thickness, and ν the Poisson ratio of the material. Unlike the length-dependent column buckling, this shell buckling result is independent of shell length. Also, the critical axial buckling load f_{cr} is independent of shell radius:

$$f_{cr} = 2\pi Rh\sigma_{cr} = \frac{2\pi Eh^2}{\sqrt{3(1-\nu^2)}}. \tag{2}$$

Thus, if single-walled nanotubes behave like cylindrical elastic shells, then shell theory predicts that they all have the same critical shell buckling load. The appropriate values of elastic constants and wall thicknesses for single-walled carbon nanotubes for use in shell theory were first determined by Yakobson et al. [11], who showed that the predictions of elastic shell theory match closely with results of atomistic buckling simulations if the values of E, h and ν are taken to be 5.5 TPa, 0.066 nm, and 0.19, respectively. In the present case, however, the nanotubes are multiwalled. In order to interpret the experimental results, shell theories for multiwalled carbon nanotubes must be used, which are not yet fully developed. The neighboring walls of a multiwalled nanotube are coupled through van der Waals interactions, which must be considered in any modified shell theory. As a first approximation, one can ignore the van der Waals force and assume that the walls are non-interacting. Then all walls buckle at the strain predicted by the shell theory for a single-walled nanotube. In this case, buckling would initiate in the outermost shell, as it has the largest radius-to-thickness ratio and thus the lowest critical buckling strain from equation 1. Using the outer radius of the multiwalled carbon nanotubes (25 nm) and the elasticity parameters of Yakobson et al. [11], the predicted critical buckling load is 1.2 μN. Thus, the non-interacting shell model predicts a critical buckling load, which is only about one half of the experimental value.

A better model was developed by Ru [12] to account for the effect of van der Waals interactions between neighboring walls. If the nanotube wall thickness is small compared to its radius, this model predicts that the critical buckling strain is the same as that of a single-walled nanotube with a radius equal to the average radius of multiwalled nanotube. Applying this theory, the critical buckling load for the nanotubes used in the current experiments can be calculated to be 1.34 μN, which is still 40% smaller than the observed value. The significant discrepancy between the predictions of the existing elastic theories and the experimental observations highlights the lack of a complete understanding of the stiffening role played by the inner walls in multiwalled nanotube mechanics. The following sections describe a possible source of this discrepancy and an analysis to account for it in calculating the critical buckling conditions.

Imperfections in Multiwalled Carbon Nanotubes

Multiwalled carbon nanotubes are rarely defect free [19]. Most multiwalled carbon nanotubes that are currently being fabricated and used in research and industry contain imperfections and consequently shear coupling between the walls. There are several kinds of defects that occur in them, such as topological defects, rehybridization defects and incomplete bonding [19]. Hybridization defects can exist in the form of sp^3 bonds between the shell walls. Apart from changing the electronic properties of the nanotubes, such inter-wall *sp3* bonds would substantially increase the inter-wall shear resistance. In contrast to the defect-free multiwalled nanotubes which are predicted to have very low sliding resistance [20], shear coupling introduced by the sp^3 bonds increases the inter-wall friction drastically. Such shear coupling will influence the mechanical behavior of the nanotubes in all those cases in which deformation involves inter-wall sliding. For example, buckling deformation of nanotube walls necessarily involves relative sliding between them; hence shear coupling is expected to increase the critical buckling load and strain of a multiwalled carbon nanotube. We propose this as a possible reason for the discrepancy between the measured buckling load and the theoretically predicted critical load noted in the previous section. Evidence for the presence of sp^3 bonds has been obtained through Raman spectroscopy experiments on the nanotubes used in the current experiments, which is presented elsewhere [21]. A detailed molecular dynamics study has been carried out by the authors [21], in which a certain percentage

of randomly located atoms form sp^3 bonds with those on the neighboring walls. Such shear coupled multiwalled nanotubes are then subjected to compressive deformation in the simulations. The results show that the percentage of atoms with sp^3 bonds have a strong effect on the critical buckling strain. Details of this computational study are reported elsewhere [21]. The objective here is to present a generalized shell buckling analysis of a multiwalled carbon nanotube in which the walls are shear coupled. Without such shear coupling, as the analysis of Ru [12] shows, the critical buckling strain of a multiwalled nanotube is same as that of a single-walled nanotube, the diameter of which is equal to the average diameter of the multiwaled nanotube. In other words, without shear coupling, having additional tubes does not increase the buckling strain. This result is in contrast with the elastic shell theory, according to which buckling strain increases linearly with the wall thickness (equation 1). This difference can be understood qualitatively as follows. An elastic continuum resists stretching deformations as well as shearing deformations (i.e., it possesses a Young's modulus and a shear modulus), whereas a defect-free multiwalled nanotube does not resist inter-wall shearing. Thus, the shear coupling introduced by the sp^3 bonds imparts a "continuum" character to the multiwalled nanotube and the critical buckling strain increases. The linear dependence of buckling strain (equation 1) on the wall thickness is an isotropic elastic continuum result, in which the shear modulus (G) is related to the Young's modulus (E) and the Poisson's ratio (ν) as $G = E/2(1+\nu)$. When a small percentage of sp^3 bonds are present, although the effective inter-wall shear modulus is non-zero, it would not follow the above isotropic relation to the in-plane Young's modulus and the Poisson's ratio. As a result, the nanotube wall can be thought of as a peculiar anisotropic material. As the percentage of sp^3 bonds increases and the nanotube wall begins to acquire more isotropic character, the buckling strain can be expected to approach the continuum result.

The scope of the analysis presented below is to model shell buckling in a multiwalled nanotube by treating each wall as an individual elastic shell, interacting with its neighboring shells through an effective shear modulus. It should be noted that the inter-wall van der Waals interactions between the walls couple the radial deflections of the walls and was considered in the analysis of Ru [12], which showed that van der Waals forces lead to conformal buckling deformation in all shells, leading to no effective enhancement in the buckling strain. Further, van der Waals interactions do not introduce any significant shear coupling.

General Shell Buckling of Shear-Coupled Multiwalled Carbon Nanotubes

Resistance to sliding between individual shells in a multiwalled carbon nanotube in the form of an effective inter-wall shear modulus will influence its deformation response under applied forces. As discussed before, such shear coupling of walls could arise from imperfections such as sp^3 bonds between atoms on neighboring walls. Since shell buckling of multiwalled nanotubes involves geometrically necessary sliding of walls with respect to each other, shear coupling is expected to increase critical buckling strain. Hence, it is necessary to develop models which can predict the effect of shear coupling on the critical buckling condition for multiwalled nanotubes. The following analysis takes into account the additional energy due to shear coupling.

Consider shell buckling of a two walled carbon nanotube under uniform axial compression in which the walls resist relative shearing or sliding. The geometry of the shell, the coordinate system used and the directions of the mid-plane displacements of the walls u, v, w are shown in Fig. 5. It is assumed that the radius of the nanotube is much greater than the spacing between the walls. Consider the deformation of a buckled two-walled nanotube, shown in Fig. 6.

For the sake of simplicity, it will be assumed for now that the radius of the nanotube is large compared to its thickness and the buckling deformation is completely conformal, i.e., the out of plane deformation w is identical in all walls. It will become evident that removing this restriction is a simple matter of algebra in the analysis and does not change the conclusions significantly.

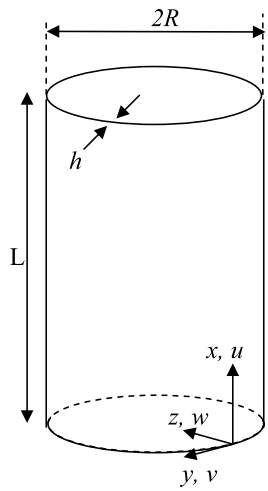

Fig. 5. Coordinate system for the shell buckling problem

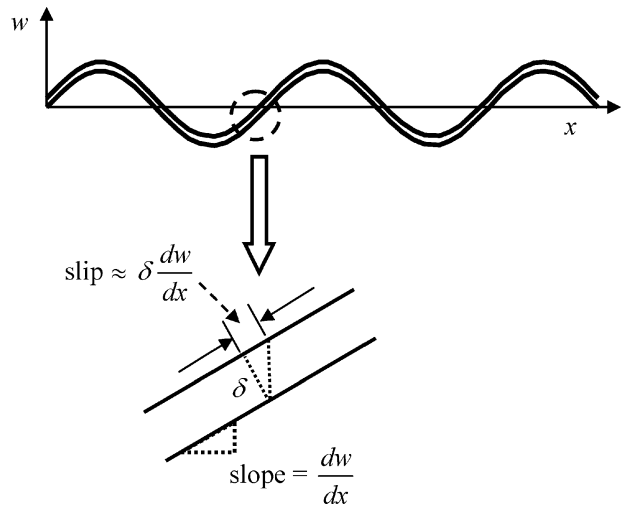

Fig. 6. Geometrically necessary relative sliding between the walls of a multiwalled carbon nanotube during buckling

When two initially parallel nanotube walls undergo the same out of plane deformation, they slide with respect to each other, as shown in Fig. 6. If δ is the spacing between the two walls and dw/dx and dw/dy are the local slopes, the relative sliding displacement s is given by

$$s = \delta\sqrt{\left(\frac{dw}{dx}\right)^2 + \left(\frac{dw}{dy}\right)^2} \tag{3}$$

Due to shear coupling, the relative sliding induces a local shear force per unit area τ on the walls, which can be approximated to be proportional to s for small values of s.

$$\tau = ks = k\delta\sqrt{\left(\frac{dw}{dx}\right)^2 + \left(\frac{dw}{dy}\right)^2} \tag{4}$$

where k is a spring constant. These quantities can also be described in the continuum parlance by defining a "shear strain" γ as

$$\gamma = \frac{s}{\delta} = \sqrt{\left(\frac{dw}{dy}\right)^2 + \left(\frac{dw}{dy}\right)^2} \tag{5}$$

and a "shear modulus" G as

$$G = \frac{\tau}{\gamma} = k\delta \tag{6}$$

Let the compressive force per unit length of circumference on each wall just prior to buckling be N_o. The corresponding pre-buckling homogeneous solution is given by

$$\varepsilon_x = \varepsilon_o = \frac{N_o}{Eh}, \quad \varepsilon_y = -\nu\varepsilon_x = -\frac{\nu N_o}{Eh} = -\nu\varepsilon_o \tag{7}$$

$$u = \varepsilon_o x, \quad v = 0, \quad w = \nu\varepsilon_o R = \frac{\nu N_o R}{Eh} \equiv w_o \tag{8}$$

Immediately following buckling, the displacement field can be assumed to be

$$\begin{aligned} u &= \varepsilon_o x + A\sin(ny/R)\cos(m\pi x/L) \\ v &= B\cos(ny/R)\sin(m\pi x/L) \\ w &= \nu\varepsilon_o R + C\sin(ny/R)\sin(m\pi x/L) \end{aligned} \tag{9}$$

which represents a buckling mode with m half wavelengths along the tube length and $2n$ half wavelengths along the circumference. m and n are integers. The constants A, B and C are small amplitudes of the buckling mode (m, n). The mid-plane strains corresponding to the above perturbed field are

$$\begin{aligned} \varepsilon_x &= u_{,x} = \varepsilon_o - A\tfrac{m\pi}{L}\sin(ny/R)\sin(m\pi x/L) \\ \varepsilon_y &= v_{,y} - \frac{w}{R} = -\nu\varepsilon_o - \frac{(Bn+C)}{R}\sin(ny/R)\sin(m\pi x/L) \\ \gamma_{xy} &= u_{,y} + v_{,x} = \left(\frac{An}{R} + \frac{Bm\pi}{L}\right)\cos(ny/R)\cos(m\pi x/L) \end{aligned} \tag{10}$$

The mid-plane curvatures are

$$\begin{aligned} \kappa_x &= w_{,xx} = -C\tfrac{m^2\pi^2}{L^2}\sin(ny/R)\sin(m\pi x/L) \\ \kappa_y &= w_{,yy} = -C\frac{n^2}{R^2}\sin(ny/R)\sin(m\pi x/L) \\ \kappa_{xy} &= w_{,xy} = C\left(\frac{n}{R}\right)\left(\frac{m\pi}{L}\right)\cos(ny/R)\cos(m\pi x/L) \end{aligned} \tag{11}$$

Adding the elastic energy due to mid-plane stretching in each wall, the total membrane elastic energy in the nanotube is

$$\begin{aligned} U_m = & 2\frac{Eh}{2(1-\nu^2)} \\ & \times \int_S \left[(\varepsilon_x + \varepsilon_y)^2 - 2(1-\nu)\left(\varepsilon_x\varepsilon_y - \frac{1}{4}\gamma_{xy}^2\right)\right] ds \end{aligned} \tag{12}$$

where S is the surface area of each wall. Using the strain expressions from equation 10, the membrane elastic energy is

$$U_m = 2\frac{Eh}{(1-\nu^2)}\left\{(1-\nu^2)\varepsilon_o^2 2\pi RL + \frac{\pi RL}{2} \times\left[\frac{A^2m^2\pi^2}{L^2} + \frac{(Bn+C)^2}{R^2} + \frac{2\pi\nu mA}{RL}(Bn+C)\right] + \frac{(1-\nu)}{4}\pi RL\left(\frac{An}{R}+\frac{Bm\pi}{L}\right)^2 - \frac{2(1-\nu^2)\varepsilon_o Am\pi}{L} \times \int_S \sin(ny/R)\sin(m\pi x/L)dS\right\} \tag{13}$$

The total elastic energy in the two walls due to bending is given by

$$U_b = 2\frac{D}{2}\int_S\left[(\kappa_x+\kappa_y)^2 - 2(1-\nu)\left(\kappa_x\kappa_y - \kappa_{xy}^2\right)\right]dS = 2C^2\frac{\pi RLD}{4}\left[\frac{m^2\pi^2}{L^2}+\frac{n^2}{R^2}\right]^2 \tag{14}$$

where equation 11 is used for curvatures. In equation 14, $D = \frac{Eh^3}{12(1-\nu^2)}$. The total stored energy due to relative sliding between the two walls or the shear coupling energy can be written as

$$U_s = \int_S \frac{1}{2}\tau\, s\, dS = \frac{1}{2}G\delta\int_S\left[\left(\frac{dw}{dx}\right)^2 + \left(\frac{dw}{dy}\right)^2\right]dS \tag{15}$$

Using the perturbed displacement w from equation 9,

$$U_s = \frac{G\delta}{4}\pi\, RL\left(\frac{m^2\pi^2}{L^2}+\frac{n^2}{R^2}\right)C^2 \tag{16}$$

The total shortening of the shells due to membrane strains and bending is

$$\Delta(y) = \int_0^L \varepsilon_x\, dx - \frac{1}{2}\int_0^L w_{,x}^2\, dx \tag{17}$$

Then, the potential energy of the applied traction can be evaluated as

$$V = 2\int_0^{2\pi R} N_o\Delta(y)dy = 4\pi RLEh\varepsilon_o^2 - \frac{1}{2L}\pi^2m^2EhR\varepsilon_oC^2 - 2\frac{Am\pi}{L}Eh\varepsilon_o\int_S \sin(ny/R)\sin(m\pi x/L)dS \tag{18}$$

The total potential energy is

$$\prod = U_m + U_b + U_s - V \tag{19}$$

Using the minimum potential energy theorem,

$$\frac{\partial\prod}{\partial A} = 0, \quad \frac{\partial\prod}{\partial B} = 0, \quad \frac{\partial\prod}{\partial C} = 0 \tag{20}$$

The first two of these three equations give

$$A = \frac{\alpha(n^2-\nu\alpha^2)}{(n^2+\alpha^2)^2}C \tag{21}$$

$$B = -\frac{n\left[n^2+(2+\nu)\alpha^2\right]}{(n^2+\alpha^2)^2}C \tag{22}$$

where

$$\alpha = \frac{m\pi R}{L} \tag{23}$$

Using these in the third of equation 20, an expression for the critical compressive strain $\varepsilon_c = -\varepsilon_o$ can be obtained as

$$\varepsilon_c = \frac{\alpha^2}{(n^2+\alpha^2)^2} + \frac{D}{EhR^2}\frac{(n^2+\alpha^2)^2}{\alpha^2} + \frac{1}{2}\frac{G\delta}{Eh}\frac{n^2+\alpha^2}{\alpha^2} \tag{24}$$

If there were no shear coupling (G = 0), this expression reduces to that of the classical shell theory result [18]. The effect of shear coupling on the critical buckling strain is explicitly through the third term in equation 24, which is also a function of the mode numbers m, n. This result can be readily generalized to an N-walled nanotube, for which, the coefficient 1/2 in the third term in equation 24 gets replaced by $(N-1)/N$. In the absence of shear coupling, the critical buckling strain is obtained by minimizing the right side of equation 24 with respect to n and α, which gives the classical shell buckling formula, equation 1. In the presence of shear coupling, by examining equation 24, it can be concluded that the minimum critical buckling strain occurs at n = 0, which is the axisymmetric buckling case and the corresponding critical buckling strain is

$$\varepsilon_c = \frac{h}{R\sqrt{3(1-\nu^2)}} + \frac{1}{2}\frac{G\delta}{Eh} \tag{25}$$

For an N-walled nanotube,

$$\varepsilon_c = \frac{h}{R\sqrt{3(1-\nu^2)}} + \frac{N-1}{N}\frac{G\delta}{Eh} \tag{26}$$

According to equation 26, the effective inter-wall shear modulus G in an imperfect multiwalled nanotube has a

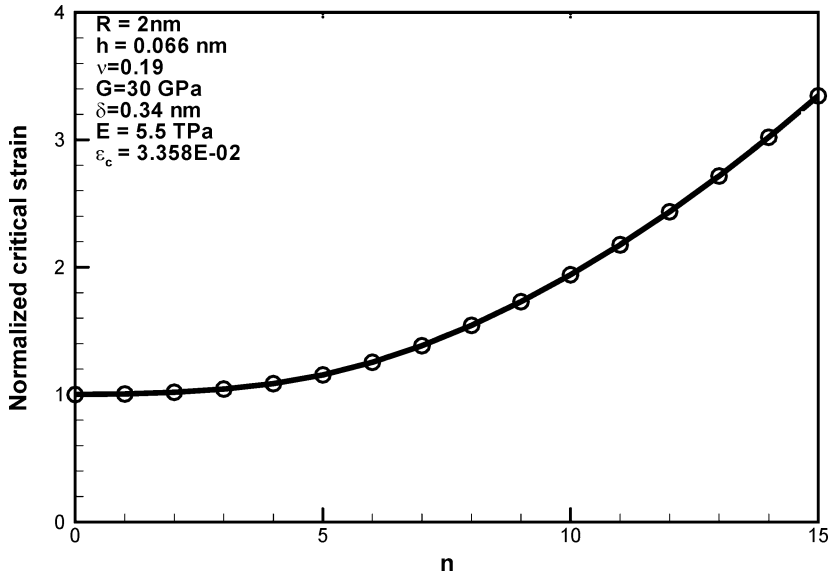

Fig. 7. Sensitivity of buckling strain to the circumferential mode number n. Note the relative insensitivity for low values of n ($n < 4$)

linear contribution to the critical buckling strain. Increasing the number of walls increases critical strain. However, the increment due to each additional wall progressively decreases; for a large number of walls, the increase in strain due to shear coupling approaches a constant value $G\delta/Eh$. Thus, equation 26 quantifies the intuitive notion that shear coupling resists buckling and bending. It also captures the trend observed in the atomistic calculations reported in [21].

From equation 24, the minimum value of the critical strain occurs for axisymmetric buckling ($n = 0$). However, atomistic calculations indicate that n is not necessarily zero and circumferential waves can appear in shear coupled nanotubes [21]. In order to understand this result, it is instructive to consider the sensitivity of buckling strain to n, by plotting equation 24, for a representative case, as shown in Fig. 7. Notice that the critical strain is insensitive to n for low values ($n \leq 3$). For $n = 3$, the critical strain is only about 4% higher than the axisymmetric case. This suggests that the axisymmetric case is *almost* as likely as $n = 1, 2, 3$ cases (2, 4 or 6 half wavelengths along the circumference).

In the current experiments, from the measured buckling load, the average critical buckling strain is 2.875×10^{-3}. The estimated value from the classical shell theory is 1.725×10^{-3}. Within the framework of the analysis, the difference between the two is due to the shear coupling term in equation 26. Using equation 26, the effective inter-wall shear modulus can be estimated as G~1.3 GPa. According to the atomistic computations [21] this value of G corresponds to about 0.25% atoms with inter-wall sp^3 bonds. Although there is no alternative and independent way to confirm this estimate, at this stage we merely note that it is a reasonable estimate.

A limitation of the analysis presented above is that it ignores the possible imperfection sensitivity of buckling strain in cylindrical shell structures, which is a well documented phenomenon [17]. It can be observed from Figs. 1 and 4 that the nanotubes tested in the experiment are not geometrically perfect structures with an ideal circular cross-section. Given the similarity of energy potentials between the nanotubes and the elastic shells, it is reasonable to expect that the former would display strong imperfection sensitivity as well. However, predictions of buckling strains from atomistic calculations agree very well with equation 1 [11, 21]. The nanotubes in these simulations are geometrically perfect and have a defect-free graphene structure. In order to understand the imperfection sensitivity in nanotubes, it is necessary to introduce geometric and other defects in the simulations. Moreover, each sp^3 bond in the imperfect nanotubes can be viewed as a defect. The increase in buckling strain observed in the experiments as well as simulations could be the net result of a positive contribution from shear coupling and a negative contribution from imperfection sensitivity. More detailed atomistic simulations and further experiments are necessary to understand the effect of shear coupling due to sp^3 bonding and imperfection sensitivity completely. Such insights can substantially change the preliminary estimate of G~1.3 GPa for the nanotubes used in the experiments.

Concluding Remarks

Experiments are reported in which individual multi-walled carbon nanotubes are subjected to uniaxial compression, and buckling loads are measured using

nanoindentation. A simple analysis has been presented to understand the discrepancy in the critical buckling load between the experimental measurements and the predictions of existing models. The analysis accounts for shear coupling between neighboring walls due to imperfections such as inter-wall sp^3 bonds. The model explains the above discrepancy and also captures the results of atomistic computations. However, it does not address the sensitivity of shell buckling strain in multi-walled nanotubes to imperfections such as deviations from circular cross-section and the presence of inter-wall sp^3 bonds, which modify the local atomic structure and hence perturb the local elastic properties. Understanding these effects is important in arriving at a coherent picture of buckling in multiwalled nanotubes. The experimental and modeling work presented here is a first step towards a more comprehensive characterization of buckling in imperfect multiwalled carbon nanotubes.

Acknowledgments The authors gratefully acknowledge useful discussions with Professor W.A. Curtin. PRG acknowledges Professor S. Suresh (MIT) for facilitating the nanoindentation experiments.

References

1. Yu MF, Files BS, Arepalli S, Ruoff RS (2000) Tensile loading of ropes of single wall carbon nanotubes and their mechanical properties. Phys Rev Lett 84:5552.
2. Yu MF, Lourie O, Dyer MJ, Moloni K, Kelly TF, Ruoff RS (2000) Strength and breaking mechanism of multiwalled carbon nanotubes under tensile load. Science 287:637.
3. Wong EW, Sheehan PE, Lieber CM (1997) Nanobeam mechanics: elasticity, strength, and toughness of nanorods and nanotubes. Science 277:1971.
4. Salvetat J-P, Briggs GAD, Bonard JM, Bacsa RR, Kulik AJ, Stöckli T, Burnham NA, Forró L (1999) Elastic and shear moduli of single-walled carbon nanotube ropes. Phys Rev Lett 82:944.
5. Treacy MMJ, Ebbesen TW, Gibson JM (1996) Exceptionally high Young's modulus observed for individual carbon nanotubes. Nature 381:6584.
6. Krishnan A, Dujardin E, Ebbesen TW, Yianilos PN, Treacy MMJ (1998) Young's modulus of single-walled nanotubes. Phys Rev B 58:14013.
7. Poncharal P, Wang ZL, Ugarte D, de Heer WA (1999) Electrostatic deflections and electromechanical resonances of carbon nanotubes. Science 283:1513.
8. Buehler MJ, Kong Y, Gao HJ (2004) Deformation mechanisms of very long single-wall carbon nanotubes subject to compressive loading. J Eng Mater-T ASME 126:245.
9. Pantano A, Boyce MC, Parks DM (2004) Mechanics of axial compression of single and multi-wall carbon nanotubes. J Eng Mater-T ASME 126:279.
10. Pantano A, Parks DM, Boyce MC (2004) Mechanics of deformation of single- and multi-wall nanotubes. J Mech Phys Solids 52:789.
11. Yakobson BI, Brabec CJ, Bernholc J (1996) Nanomechanics of carbon tubes: instabilities beyond linear response. Phys Rev Lett 76:2511.
12. Ru CQ (2001) Degraded axial buckling strain of multiwalled carbon nanotubes due to interlayer slips. J Appl Phys 89:3426.
13. Dong L, Arai F, Fukuda T (2004) Destructive constructions of nanostructures with carbon nanotubes through nanorobotic manipulation. IEEE Trans Mechatronics 9:350.
14. Waters JF, Riester L, Jouzi M, Guduru PR, Xu JM (2004) Observations of compression instabilities in multi-walled carbon nanotubes. Appl Phys Lett 85:1787–1789.
15. Waters JF, Guduru PR, Hanlon T, Jouzi M, Xu JM, Suresh S (2005) Shell buckling of individual multi-walled carbon nanotubes using nanoindentation. Appl Phys Lett 87:103109.
16. Li J, Papadopoulos C, Xu JM, Moskovits M (1999) Highly-ordered carbon nanotube arrays for electronics applications. Appl Phys Lett 75:367.
17. Singer J, Arbocz J, Weller T (2002) Buckling experiments: experimental methods in buckling of thin-walled structures, volume 2. Wiley, New York.
18. Timoshenko SP, Gere JM (1961) Theory of elastic stability. McGraw-Hill, New York.
19. Ebbesen TW, Takada T (1995) Topological and sp^3 defect structures in nanotubes. Carbon 33:973–978.
20. Guo WL, Gao HJ (2005) Optimized bearing and interlayer friction in multiwalled carbon nanotubes. Comp Model Eng Sci 7:19–34.
21. Xia Z, Guduru PR, Curtin WA (2005) Buckling and load transfer of multi-wall carbon nanotubes with sp^3 intertube bridging. Submitted to *Physical Review*.